Eur. Phys. J. A **25**, s01, 403–408 (2005)
DOI: 10.1140/epjad/i2005-06-188-7

EPJ A direct
electronic only

Spectroscopy on neutron-rich nuclei at RIKEN

Hiroyoshi Sakurai[a]

Department of Physics, University of Tokyo, 7-3-1 Hongo, Bunkyo-ku, Tokyo 113-0033, Japan

Received: 14 December 2004 /
Published online: 11 August 2005 –

Abstract. Recent studies on nuclear structure by using radioactive isotope beams available at the RIKEN projectile-fragment separator (RIPS) are introduced. Special emphasis is given to experiments selected from recent programs that highlight studies; the particle stability of very neutron-rich nuclei, ^{34}Ne, ^{37}Na and ^{43}Si, the nuclear structure of ^{27}F, ^{30}Ne and ^{34}Si at $N \sim 20$, and the anomalous quadrupole transition in ^{16}C.

PACS. 21.10.Dr Binding energies and masses – 23.20.-g Electromagnetic transitions – 23.20.Lv γ transitions and level energies – 25.60.-t Reaction induced by unstable nuclei – 29.30.Kv X- and γ-ray spectroscopy

1 Introduction

Radioactive isotope (RI) beams, bringing out a high isospin degree of freedom, have given a great opportunity to investigate nuclei far from stability and to reveal out new phenomena under extreme conditions of isospin asymmetry. Experimental programs at the RIKEN projectile fragment separator (RIPS) [1] have demonstrated such potentials of RI beams. Intensities of fast RI beams available at the RIPS are at the world-highest level in the light mass region. This situation has been realized by combination of the RIPS and the high energy and intense primary beams. The RIPS has large momentum and angular acceptances as well as a sizable maximum magnetic rigidity, hence has a high collecting power of projectile fragments. The intense RI beams have made it possible to use secondary nuclear reactions for studies of the nuclear structure, and unique spectroscopic methods and techniques are being developed to obtain exotic properties of unstable nuclei.

In this report, we introduce recent highlights of experimental programs at RIKEN for last three years. Recently the RIKEN Accelerator Research Facility (RARF) has been upgraded in concert with a new project, RI Beam Factory (RIBF) [2], as introduced in sect. 2. A new injection scheme has been developed according to additional accelerator equipments installed at the RARF, and being used to deliver more intense primary beams than before. One of highlights in experimental programs based on the new acceleration scheme is presented in sect. 3. To overcome experimental difficulties stemming from low yield rates, we developed a liquid hydrogen/deuterium target. This target is useful to access nuclei very far from the stability line, and has been intensively used for studies of the nuclear structure via the in-beam γ spectroscopy. Some of highlights for $N \sim 20$ nuclei are shown in sect. 4. To study nuclear collectivity in the light mass region, new experimental techniques in terms of the in-beam γ spectroscopy have been developed and applied for the ^{16}C nucleus. In sect. 5, results of three experimental programs are shown and discussed.

[a] Conference presenter;
e-mail: sakurai@phys.s.u-tokyo.ac.jp

2 Recent upgrades of RIKEN facility

Combination of the accelerator facility existing and a new facility being constructed will deliver intense heavy-ion beams for RI productions at the RIBF, as shown in fig. 1 [2]. The accelerator complex in the present facility consists of the RIKEN Ring Cyclotron (RRC) and two injectors; the AVF cyclotron and RIKEN heavy-ion linear accelerator (RILAC). The RILAC and RRC will be used as injectors for two post-accelerators in the new facility; the Intermediate stage Ring Cyclotron (IRC) and the Super-conducting Ring Cyclotron (SRC). To provide powerful primary beams for the post-accelerators, additional accelerator devices were installed at the RILAC; an 18GHz ECR ion source, an RFQ and a booster system called the Charge-state multiplier (CSM).

Based on the upgraded RILAC, a new acceleration scheme for the RRC has been developed to obtain intense primary beams at the RIPS. An alternative injection scheme, which is often employed to have higher-energy beams, is by use of the AVF cyclotron. The new acceleration scheme with the RILAC can provide much more intense primary beams than the AVF injection. For instance,

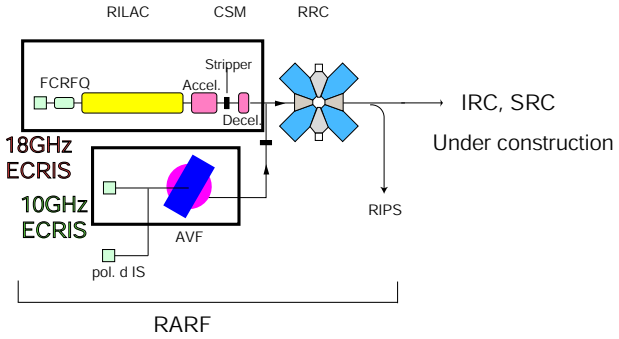

Fig. 1. A schematic layout of the present RIKEN Accelerator Research Facility (RARF).

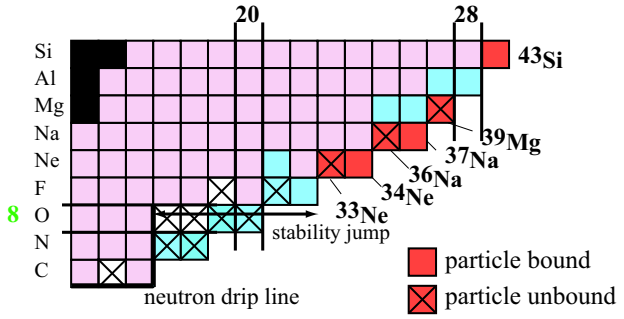

Fig. 2. New neutron-rich isotopes found at RIKEN. ^{34}Ne, ^{37}Na and ^{43}Si are found particle stable, while evidence on particle instability of ^{33}Ne, ^{36}Na and ^{39}Mg is obtained.

a typical beam intensity of ^{48}Ca is 4 pnA by the AVF injection, and 150 pnA by the RILAC injection. Differences of beam energy at the RRC between the two schemes are small for neutron-rich stable isotopes; 70A MeV for ^{48}Ca via the AVF injection and 63A MeV via the RILAC injection. Thus, the RILAC injection has given 30 times higher production rates of RI beams than the AVF injection. The RILAC scheme also delivers a 64A MeV ^{86}Kr beams with an intensity of 100 pnA at maximum.

Combination of the RIPS and the powerful primary beams accelerated via the new injection scheme has provided further opportunities to proceed towards the neutron-drip line. Several experimental programs by use of the powerful primary beams have been already performed; to search for new neutron-rich isotopes [3] and to study the nuclear structure via the in-beam γ spectroscopy [4,5,6].

3 Particle stability at N = 20–28

The experiment searching for new isotopes by using the ^{48}Ca beam [3] is introduced as one of experimental programs using the powerful beams realized by the new acceleration scheme, as described in the previous section.

The neutron-rich stable isotope ^{48}Ca is a major source to produce extremely neutron-rich nuclei up to $Z \sim 20$ and $N \sim 28$ via the projectile fragmentation reaction. The ^{48}Ca beam reacted with a ^{181}Ta target and the reaction fragments were collected and analyzed with the RIPS. Two different settings of the magnetic rigidity ($B\rho$) were employed to search for new isotopes; one optimized for ^{40}Mg and the other for ^{43}Si. Particle identification was performed event by event by a standard method on the basis of TOF-ΔE-E-$B\rho$ measurements. Further details of the experimental setup are found in ref. [3].

We observed for the first time three new isotopes, ^{34}Ne, ^{37}Na and ^{43}Si. The ^{33}Ne, ^{36}Na and ^{39,40}Mg isotopes were not observed in this experiment. According to the systematic behaviors of the production cross sections for the observed isotopes, the expected cross sections for the ^{33}Ne, ^{36}Na and ^{39}Mg isotopes were obtained to be about 10, 3, and 1 pb, respectively. The 1 pb cross section corresponds to about 30 events for ^{39}Mg at the ^{40}Mg $B\rho$ setting. Thus, the absence of events of ^{33}Ne, ^{36}Na and ^{39}Mg clearly deviates from the expectation and provides a proof for the particle unbound character of ^{33}Ne, ^{36}Na and ^{39}Mg. The expected cross section for ^{40}Mg is an order of 0.01 pb. One event observation of ^{40}Mg at the ^{40}Mg $B\rho$ setting corresponds to about 0.03 pb, which gives the detection limit of the experiment. Therefore, the question whether ^{40}Mg is particle bound or not is left for a future attempt requiring a higher luminosity.

In this work, the heaviest isotopes of Ne, Na and Si have been extended to ^{34}Ne, ^{37}Na and ^{43}Si, and particle instability of ^{33}Ne, ^{36}Na and ^{39}Mg has been found, as illustrated in fig. 2. These findings are rather in good agreement with the recent mass formula [7]. Concerning the stability of ^{43}Si, two mass formulas, FRDM [7] and ETFSI [8], disagree each other. The FRDM predicts instability with $S_{\rm n} = -1.68$ MeV, while the ETFSI does stability. A major difference between the two formulas lies in the degree of deformation. The ETFSI predicts a larger deformation than the FRDM for the silicon isotopes at $N \sim 28$. Recent shell models and mean field calculations, cited in ref. [3], have also predicted a possible deformation of a nearby nucleus ^{42}Si. Thus, the particle stability found for ^{43}Si may be attributed to a deformation effect. A recent half-life measurement for ^{42}Si has also suggested the possible deformation at $N = 28$ [9].

4 Neutron-rich nuclei at N ∼ 20

Since 1970s, a spot of the nuclear chart at $Z \sim 11$ and $N \sim 20$, the so-called "island-of-inversion" region, has been investigated with respect to the magicity loss at $N = 20$. According to recent developments of RI production methods at both ISOL and in-flight facilities, RI production rates in this region have been drastically increased, and secondary reactions have been applied to study the nuclear structure.

One of spectroscopic methods based on reactions is the in-beam γ spectroscopy. Since the intermediate-energy Coulomb excitation was applied for ^{32}Mg to obtain a $B(E2)$ value [10], several reactions and experimental techniques dedicated for fast RI beams have been developed and applied to nuclei in the island-of-inversion region. "Cocktail" beams containing a bunch of nuclei of interest have led to efficient production of data on $B(E2)$ for

neutron-rich nuclei at $N = 20$–28 [11]. The projectile fragmentation reaction with primary beams has been possible to obtain information on higher spin and excited states, compared with the Coulomb excitation [12]. The fragmentation reaction with fast RI beams instead of primary beams, the so-called two step fragmentation, has given a larger access to nuclei far from the stability line [13]. The two-nucleon knock-out reaction has been recently developed and applied for ^{32}Mg [14].

Further efforts at RIKEN have been made to obtain new information by developing new techniques in the in-beam γ spectroscopy. For the Mg isotopes beyond $N = 20$, two experimental works for ^{34}Mg were performed; the two step fragmentation [13] and the Coulomb excitation [15]. The two experiments showed that ^{34}Mg has a larger deformation than ^{32}Mg. To find whether and how deformation evolves in the isotopes with a lower Z along $N = 20$, increase of luminosity by enhancement of number of target nuclei should be desirable, since the beam intensity of ^{30}Ne is one order of magnitude lower than that of ^{34}Mg. To overcome the low beam intensity, we developed a liquid hydrogen/deuterium target at RIKEN [16].

In this section, we present results of three experiments with the liquid hydrogen/deuterium target [16]. Two of them using the proton inelastic scattering have found excited states of ^{30}Ne and ^{27}F [17,18]. The other experiment with the deuterium target is to study for ^{34}Si [19], where multitudes of excited states were populated and γ-γ coincidence technique was employed. One of the experiments [18] utilized a new NaI setup for γ detection, called DALI2 [20], while the other experiments used an old NaI setup (DALI) [10]. Compared with the DALI, the DALI2 was designed to have higher detection efficiency by larger angular coverage and higher angular resolution due to higher segmentation.

4.1 ^{30}Ne

To determine energies of first excited states ($E(2_1^+)$) for even-even isotopes is essential for understanding the nuclear structure and collectivity. The experimental finding of $E(2_1^+)$ for ^{30}Ne was performed by using the liquid hydrogen target [17].

The neutron-rich isotope ^{30}Ne was produced via a primary ^{40}Ar beam of 95 A MeV with a typical intensity of 60 pnA, which bombarded a ^{181}Ta target. The beam was accelerated via the AVF injection scheme (sect. 2). Particle identification was made by measuring event by event the energy loss, time of flight, and magnetic rigidity. Horizontal positions of the fragments at the momentum dispersive focal plane of RIPS (F1) were measured to determine the $B\rho$ values using a parallel plate avalanche counter (PPAC) [21]. The $B\rho$ measurement is essential to have the maximum intensity of ^{30}Ne at the RIPS. To identify $A = 30$ fragments without the $B\rho$ measurement, the momentum acceptance should be limited to $1/A$, namely, less than 3%, while the $B\rho$ measurement allows us to set the momentum acceptance of RIPS at maximum (6%).

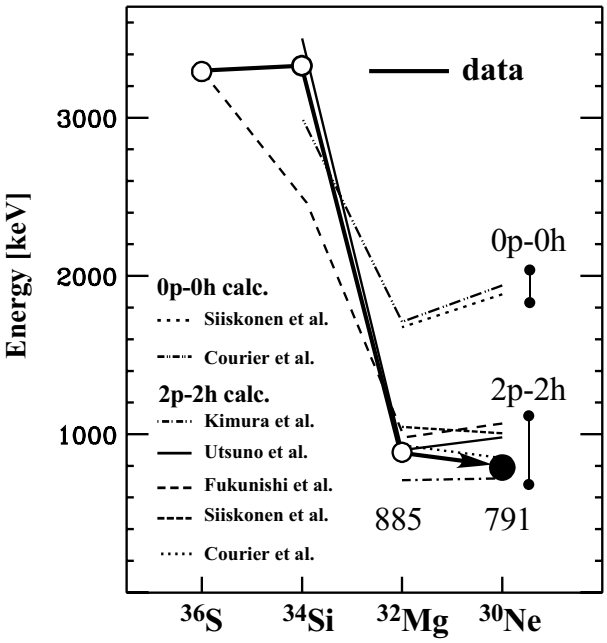

Fig. 3. Energies of the first 2^+ states in even-even $N = 20$ isotones (circles) together with theoretical predictions (from ref. [17]). The theoretical works cited are found in ref. [17].

The PPAC used at F1 is a delay-line readout type for position determination, hence giving a large tolerance under high rate circumstance and a wide dynamic range for Z of fragments. The mean intensity of the ^{30}Ne beam was about 0.2 particles per second, and the purity was 6.7%. The liquid hydrogen target was placed at the final focus of RIPS to excite the projectile. The thickness of the hydrogen target cell was 186 mg/cm^2 on average. The average energy of ^{30}Ne at the center of the target was estimated to be 48 A MeV. Identification of Z for ejectiles was made by the TOF-ΔE method, by using a PPAC and a silicon telescope. Other details of the experimental setup are found in ref. [17].

Doppler-corrected energy spectrum of γ-rays for the ^{30}Ne beam was found to have a significant γ-line at 791(26) keV. The corresponding cross section of the 791 keV transition was evaluated to be 30 ± 18 mb. By use of a coupled channel calculation and a phenomenological optical potential, the deformation parameter of $\beta_{\mathrm{pp'}}$ was obtained to be ~ 0.58. Under the assumption that electromagnetic deformation is the same as for (p, p′) scattering, the reduced $E2$ transition probability $B(E2; 0^+ \rightarrow 2^+)$ was estimated to be $\sim 460\,\mathrm{e^2fm^4}$. Details of analysis procedures are found in ref. [17].

This result for ^{30}Ne is compared to $E(2_1^+)$ values measured for neighboring $N = 20$ isotones together with theoretical predictions, as cited in fig. 3. The measured $E(2_1^+)$ values for ^{30}Ne and ^{32}Mg are considerably smaller than for other $N = 20$ isotones. The energy of 791 keV obtained for ^{30}Ne is even smaller than that of ^{32}Mg (885 keV), suggesting a larger deformation for ^{30}Ne. Theoretical predictions as cited in fig. 3 [17] are categorized into two groups as $0p$-$0h$ and $2p$-$2h$ models across $N = 20$. Obviously shown

in this figure, the experimental value of $E(2_1^+)$ for ^{30}Ne favors $2p$-$2h$ models, and suggesting that the ^{30}Ne nucleus belongs to the island-of-inversion region.

4.2 ^{27}F

One interesting question related to the island-of-inversion region is the extra-enhancement of binding energies for heavy fluorine isotopes. The heaviest fluorine isotope observed so far is ^{31}F while that for oxygen is ^{24}O [21]. It is remarkable that at least six additional neutrons can be bound by moving from oxygen to fluorine. Based on mass information for nuclei in the island-of-inversion region [22], extra-enhancement of their binding energies has been observed as one of exotic features. This enhancement may be due to deformation effects manifested in this region. To understand mechanism of the bound nature of ^{31}F, a key issue is magnitude of deformation for the heavy fluorine isotopes. As presented in the previous subsection, ^{30}Ne is suggested to have a larger deformation than ^{32}Mg. One may ask further whether the fluorine isotopes at $N \sim 20$ have a larger deformation than ^{30}Ne or not. To answer this question, the bound states of ^{27}F have been searched for [18]. Their existence or energies would provide useful information on the magnitude of deformation.

γ-lines were searched for p(^{27}F, ^{25,26,27}F) channels. Doppler corrected energy spectrum of γ-rays for each channel showed two γ-lines originated from each ejectile. The ^{27}F spectrum was found to have the γ-lines at 504(15) and 777(19) keV of which statistical confidences are 2.4 and 3.0 σ, respectively. The experimental cross sections for the γ-ray transitions are σ(504 keV) = 11.0±5.0 mb and σ(777 keV) = 18.0±6.0 mb. The other γ-lines found for ^{25}F (^{26}F) are at 727(22) and 1753(53) keV (468(17) and 665(12) keV). All the above bound states have been observed for the first time.

The existence of the bound excited states in ^{27}F suggests a significant deformation for ^{27}F. An *sd*-shell model predicts that the first excited state of $1/2^+$ is located at about 2 MeV [23], which is beyond the particle threshold of ^{27}F(S_n = 1.4 MeV). This prediction is obviously contradictory on the experimental findings. On the other hand, an *spdf*-shell model calculation [24] leads to the melting of $N = 20$ shell gap and hence predicting the $1/2^+$ energy of about 1 MeV. According to this shell model work, when one moves to a lower Z along $N = 20$, collectivity becomes larger due to a larger fraction of $4p$-$4h$ configuration. It is interesting to note that the energy observed for the excited state (777 keV) is even lower than that predicted (1 MeV), suggesting that ^{27}F may have a larger deformation than predicted. More elaborated theoretical works are necessary to understand mechanism for the low-lying excited state in ^{27}F.

4.3 ^{34}Si

The nuclear structure of ^{34}Si is interesting in terms of a shape coexistence proposed, hence a deformed 0_2^+ state with the $2p$-$2h$ intruder configuration has been searched for. Recently, an experimental work via ^{34}Al β-γ spectroscopy found several γ lines [25]. Three of them at 1.193, 1.715 and 2.696 MeV were not placed in ^{34}Si. In addition, it was suggested that the 1193 keV γ line observed is the candidate of $2_1^+ \rightarrow 0_2^+$ transition. To clarify the nature of these unplaced γ lines and to examine the suggestion of the 0_2^+ state, deuteron inelastic scattering of ^{34}Si was studied [19].

High statistics given by the liquid deuterium target enabled us to perform γ-γ coincidence. Doppler-corrected γ energy spectrum was obtained in coincidence with the 3.326 MeV γ-rays corresponding to the $2_1^+ \rightarrow 0_1^+$ transition. In this spectrum, four γ lines at 0.930, 1.193, 1.715 and 2.696 were found to be associated with the 3.326 MeV γ-rays. In addition, all the transitions corresponding to the γ lines were found to feed finally the 2_1^+ state with almost 100% probability. According to the experimental facts, a level scheme of ^{34}Si was constructed [19]. It was also indicated that the possible existence of the 0_2^+ state at 2.133 MeV is unlikely. Further experimental efforts have to be made to search for the 0_2^+ state for future.

5 Anomalous quadrupole collectivity in ^{16}C

One of the important $E2$ transitions in an even-even nucleus is that from the first 2^+ state to the ground state. The reduced transition probability $B(E2)$ for the transition has long been a basic observable in the extraction of the magnitude of nuclear collectivity or in probing anomalies in the nuclear structure. With the recent advance of the intermediate energy Coulomb excitation, the magicity has been examined over the nuclear chart through measurements of $E2$ strengths [10]. In the light mass region of $Z < 8$, however, the Coulomb excitation may suffer from contamination of nuclear excitation. Thus, new experimental techniques were desired to deduce $B(E2)$ values for the light mass region.

To obtain the $B(E2)$ information, we have developed a new technique applied for the ^{16}C isotope, where lifetime of an excited state is measured with fast RI beams. This experiment has shown an anomalously hindered $B(E2)$ [26]. Alternatively, the Coulomb-nuclear interference method has given a large difference of proton and neutron transition matrix elements [27]. In addition to the proton collectivity deduced from $B(E2)$, magnitude of neutron collectivity has been studied via the proton inelastic scattering [28], which is the most neutron sensitive reaction. Results of the three experiments based on the in-beam γ spectroscopy are presented and possible mechanism of the anomaly would be discussed.

5.1 Recoil shadow method

The electric quadrupole transition from 2_1^+ to $0_{\rm g.s.}^+$ in ^{16}C was studied through measurement of the lifetime for the 2_1^+ state by a recoil shadow method [26]. In this method, an emission point of the de-excitation γ-ray is located and

the γ-ray intensity is recorded as a function of the flight distance of the de-exciting nucleus. As the flight velocity of the de-exciting nucleus is close to half the velocity of light, the flight distance over 100 ps corresponds to a macroscopic length of about 1.7 cm. Experimental observables reflecting lifetime were γ-ray yields recorded at two NaI rings located around a target, of which acceptances were geometrically determined with respect of a lead slab around the target and the emission point. Thus, yield ratios between the two rings had lifetime dependence. Details of the experimental setup and analysis procedures are found in ref. [26].

The adopted value for the lifetime is 77 ± 14(stat) ± 19(syst) ps. The central value corresponds to the $B(E2; 2^+ \rightarrow 0^+)$ value of 0.63 $e^2\mathrm{fm}^4$ or 0.26 in Weisskopf units (W.u.). The systematic error was deduced by taking into account two major sources; geometrical uncertainty, optical potential dependences of the angular distribution of γ-ray emission. It should be noted that the γ-ray yield measurement was conducted at two target positions to examine validity of this method.

The $B(E2)$ value obtained for ^{16}C was compared with all the other $B(E2)$ values known for the even-even nuclei with $A \leq 50$ [26]. Nuclei with open shells tend to have $B(E2)$ values greater than 10 W.u., whereas nuclei with shell closure of neutrons or protons tend to have distinctly smaller $B(E2)$ values. Typical examples of the latter category are doubly magic nuclei, ^{16}O and ^{48}Ca, of which $B(E2)$ values are 3.17 and 1.58 W.u., respectively. The value of $B(E2)$ for ^{16}C is even smaller than these extreme cases by as much as an order of magnitude.

Comparison of the $B(E2)$ value with an empirical formula based on a quantum liquid-drop model [29] illustrates the anomalously strong hindrance of the transition. The experimental $B(E2)$ value for ^{16}C relative to that predicted by the formula is 0.036, which is exceptionally small, far smaller than for any other nuclei, including closed-shell nuclei.

5.2 Coulomb-nuclear interference method

The neutron and proton quadrupole excitations in ^{16}C were investigated by use of the Coulomb-nuclear interference method applied to the $^{208}\mathrm{Pb} + {}^{16}\mathrm{C}$ scattering. To observe the interference pattern in angular distribution of the ^{16}C nuclei for the inelastic channel, a high angular resolution of 0.28°(r.m.s.) was achieved in this experiment. A thin Pb target with a thickness of 50 mg/cm^2 was used to minimize the multiple-scattering effect, and four PPACs with a position resolution of 0.2 mm (r.m.s.) were employed for the scattering angle measurement [27].

The obtained differential cross section was analyzed with the standard coupled channel code and two sets of optical potentials [27]. Parameters of the Coulomb deformation length δ_C and the matter deformation length δ_M were obtained from the best fit of the data. There were two χ^2-minima for $\delta_\mathrm{M}/\delta_\mathrm{C}$. The ratio giving a better χ^2 was 3.1. Combination of the ratio with Bernstein's prescription [30] leads to a ratio of the neutron and proton matrix elements, $M_\mathrm{n}/M_\mathrm{p}$ of 7.6 ± 1.7. The $M_\mathrm{n}/M_\mathrm{p}$ ratio is larger than N/Z =1.67 that would be expected for a purely isoscalar transition.

By normalizing the absolute cross section, the absolute values for δ_C and δ_M were deduced to be 0.42 ± 0.05 and 1.3±0.15 fm, respectively. The corresponding $B(E2)$ value was 0.28 ± 0.06 W.u., consistent with the lifetime measurement [26].

5.3 Proton inelastic scattering

The $B(E2)$ value obtained through the lifetime measurement of the 2_1^+ state in ^{16}C was found to be remarkably small. This finding raises an intriguing question as to whether or not the neutron contribution is similarly small for the relevant quadrupole transition. To answer this question, a study using a proton probe sensitive to neutrons, namely via the inelastic proton scattering, was performed. In this experiment, the in-beam γ spectroscopy was used in inverse kinematics [31]. Ingredients of this experiment are use of the liquid hydrogen target [16] and the new NaI setup DALI2 [20]. These equipments enhanced the feasibility of this method. More information on the experimental setup is found in ref. [28].

The deformation parameter $\beta_{\mathrm{pp}'}$ was obtained to be 0.50(8) from the measured angular-integrated cross section of 24.1 mb. This deformation parameter was found to be significantly larger than that of the lifetime measurement (0.14). Combination of the result of the lifetime measurement [26] with Bernstein's prescription gives us a ratio of the neutron and proton quadrupole matrix elements $(M_\mathrm{n}/M_\mathrm{p})/(N/Z)$ of 4.0 ± 0.9 [28], which is in good agreement with the result obtained by the Coulomb-nuclear interference [27].

5.4 Discussion

The three experiments for the quadrupole transition in ^{16}C have provided the results consistent with each other, and strengthening the fact of the anomaly of $B(E2)$ in ^{16}C.

To find a possible mechanism for understanding the anomaly, two experimental facts observed in the neighboring nuclei are emphasized. The first one is proton and neutron shell gaps in the light mass region, which can be deduced from the mass information. The proton (neutron) shell gaps G_p (G_n) are calculated through the following empirical formulas; $G_\mathrm{p} = S_{2\mathrm{p}}(Z,N) - S_{2\mathrm{p}}(Z+2,N)$ and $G_\mathrm{n} = S_{2\mathrm{n}}(Z,N) - S_{2\mathrm{n}}(Z,N+2)$. The values of $S_{2\mathrm{p}}$ and $S_{2\mathrm{n}}$ are taken from ref. [22]. The values of the shell gaps are shown in fig. 4. A region of $6 \leq Z \leq 8$ and $10 \leq N \leq 13$ has a small value of G_n, less than about 1 MeV, and showing a "degeneracy" of *sd*-shell for neutron orbitals. On the other hand, the G_p values in this region are about 10 MeV. As for ^{16}C, the value of G_n is as small as 0.6 MeV, while that of G_p is as large as 12 MeV. This remarkable contrast of shell gaps between protons and neutrons may depict a hard proton matter and a soft neutron matter of

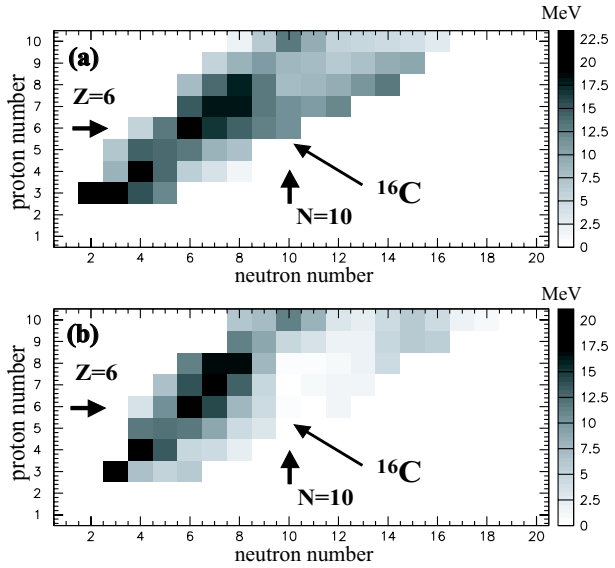

Fig. 4. Shell gaps calculated for protons (a) and for neutrons (b), by using the nuclear mass compilation [22].

nuclei in this region. The second fact to be noted is magnitude of the effective charges for neutrons. Measurement of electric quadrupole moments for ^{15,17}B [32] suggests that the $E2$ effective charges can be remarkably reduced for the neutron-rich nuclei. According to the two observation, the hard proton core and the valence neutrons degenerating with the small effective charges give qualitatively a small $B(E2)$ value. Quantitative predictions based on microscopic models are found and cited in refs. [26,27].

These discussions raise a next question: how the anomalous $B(E2)$ region is extended toward a larger N and what underlying mechanism causing the asymmetric dynamics between protons and neutrons is. To answer these questions, further experimental studies on neighboring nuclei as well as theoretical attempts would be necessary.

6 Summary

It has been demonstrated that the new spectroscopic information has been obtained by means of the new spectroscopic techniques developed for fast RI beams, which illustrate the activities at the RIKEN-RIPS and potentials of fast RI beams.

Before the new facility RIBF constructed, the present accelerator facility has been upgraded and several experiment programs have been performed by use of intense primary beams, such as ^{40}Ar, ^{48}Ca and ^{86}Kr. The methods and techniques developed at the RIKEN-RIPS will be naturally extended to experimental programs at the RIBF to investigate heavier or more neutron-rich nuclei than available at the present facility. The two accelerators IRC and SRC and a new RI beam separator Big-RIPS are being constructed. In 2007, RI beams will be delivered for experimental programs at the RIBF.

This work described here represents the efforts of many people, whom I have tried to adequately reference. In particular, most of the experiments presented here were performed in collaboration with University of Tokyo, Rikkyo University and RIKEN. The experiment for particle stability [3] was undertaken with University of Tokyo, JINR and RIKEN collaboration. A few experiments [18,27,28] were under the ATOMKI-RIKEN collaboration.

References

1. T. Kubo *et al.*, Nucl. Instrum. Methods B **70**, 309 (1992).
2. `http://www.rarf.riken.go.jp/RIBF/overview-e.htm`.
3. M. Notani *et al.*, Phys. Lett. B **542**, 49 (2002) and references therein.
4. S. Michimasa *et al.*, these proceedings, p. 367.
5. H. Iwasaki *et al.*, these proceedings, p. 415.
6. E. Ideguchi *et al.*, these proceedings, p. 429.
7. P. Möller *et al.*, At. Data Nucl. Data Tables **39**, 185 (1995).
8. Y. Aboussir *et al.*, At. Data Nucl. Data Tables **61**, 127 (1995).
9. S. Grévy *et al.*, Phys. Lett. B **594**, 252 (2004).
10. T. Motobayashi *et al.*, Phys. Lett. B **346**, 9 (1995).
11. T. Glasmacher *et al.*, Phys. Lett. B **395**, 163 (1997).
12. F. Azaiez *et al.*, Eur. Phys. J. A **15**, 93 (2002).
13. K. Yoneda *et al.*, Phys. Lett. B **499**, 233 (2001).
14. D. Bazin *et al.*, Phys. Rev. Lett. **91**, 012501 (2003).
15. H. Iwasaki *et al.*, Phys. Lett. B **522**, 227 (2001).
16. H. Akiyoshi *et al.*, RIKEN Accel. Prog. Rep. **32**, 167 (1999).
17. Y. Yanagisawa *et al.*, Phys. Lett. B **566**, 84 (2003) and references therein.
18. Z. Elekes *et al.*, Phys. Lett. B **599**, 17 (2004).
19. N. Iwasa *et al.*, Phys. Rev. C **67**, 064315 (2003).
20. S. Takeuchi *et al.*, RIKEN Accel. Prog. Rep. **32**, 148 (2003).
21. H. Sakurai *et al.*, Phys. Lett. B **448**, 180 (1999).
22. G. Audi, A.H. Wapstra, C. Thibault, Nucl. Phys. A **729**, 337 (2003).
23. B.A. Brown, `http://www.nscl.msu.edu/sde.htm`.
24. Y. Utsuno *et al.*, Phys. Rev. C **64**, 011301(R) (2001).
25. S. Nummela *et al.*, Phys. Rev. C **63**, 044316 (2001).
26. N. Imai *et al.*, Phys. Rev. Lett. **92**, 062501 (2004).
27. Z. Elekes *et al.*, Phys. Lett. B **586**, 34 (2004).
28. H.J. Ong *et al.*, these proceedings, p. 347.
29. S. Raman *et al.*, Phys. Rev. C **37**, 805 (1988).
30. A.M. Bernstein *et al.*, Commun. Nucl. Phys. **11**, 203 (1983).
31. H. Iwasaki *et al.*, Phys. Lett. B **481**, 7 (2000).
32. H. Izumi *et al.*, Phys. Lett. B **366**, 51 (1996); H. Ogawa *et al.*, Phys. Rev. C **67**, 064308 (2003).